Journal of Applied Fluid Mechanics, Vol. 18, No. 5, pp. 1349-1363, 2025.
Available online at www.jafmonline.net, ISSN 1735-3572, EISSN 1735-3645.
https://doi.org/10.47176/jafm.18.5.2958

Investigation of Wing Lift Enhancement by Combination of Plasma Jet Actuator and Synthetic Jet Actuator

N. Ding[1,2], F. Gao[2], C. Tang[3] and J. Chang[1,2†]

[1] *College of Mechatronics Engineering, North University of China, Taiyuan 030051, China*
[2] *Research Institute of Intelligent, North University of China, Taiyuan 030051, China*
[3] *Jinxi Industrial Group Co.,Ltd, Taiyuan 030051, China*

†*Corresponding Author Email: changjl@nuc.edu.cn*

ABSTRACT

In order to improve the aerodynamic characteristics and maneuverability of fixed-wing UAV, an improved method to enhance the wing lift by the combination of plasma jet actuator and synthetic jet actuator based on active flow control technique is presented. The aerodynamics of the wing under flow control are calculated by fluent hydrodynamics software. Firstly, the effects of different control modes on the aerodynamic characteristics are compared, including single PJA control, single SJA control, combined PAS control and combined SAP control modes. Lift enhancement mechanism in combined control mode and the advantages are analyzed. Secondly, the effects of flow control parameters, involving the plasma discharge voltage, the maximum exit velocity of the synthetic jet and the deflection angle on the aerodynamic characteristics are investigated in detail. The results show that installing a flow control device at the leading edge of the aileron can substantially increase the lift of both the main wing and aileron when using the PAS flow control mode. The main wing lift is the primary contributor to the total lift increase, accounting for up to 79% of the total lift increase. The hysteresis phenomenon of the pressure recovery on the surface of the main wing is one of the main reasons for the total lift to remain at a high level. Meanwhile, raising the plasma voltage can steadily increase the lift of the wing, while raising the exit velocity of the synthetic jet can cause more lift fluctuations while increasing the lift.

Article History

Received July 7, 2024
Revised December 6, 2024
Accepted January 15, 2025
Available online March 4, 2025

Keywords:

Synthetic jet actuator
Plasma jet actuator
UAV
Lift coefficient
Flow control

1. INTRODUCTION

With the advancement of science and technology, the use of unmanned aerial vehicles (UAV), commonly known as drones, is becoming increasingly common. In the civilian field, UAVs are capable of performing tasks such as agricultural irrigation, forest search and rescue, and firefighting. In the military field, UAVs are able to realize multi-copter cooperative operations and perform tasks such as reconnaissance, jamming and network relay. Among them, there are the advantages such as high speed, long range and large payload capacity in fixed-wing UAVs, which are more adaptable to the future battlefield environment. In recent years, fixed-wing UAVs have been extensively studied by scientists (Shakhatreh Elmeseiry McEnroe).

Effectively increasing and sensitively controlling wing lift is one of the primary methods to enhance the performance of fixed-wing UAVs. By increasing the lift of the UAV, greater efficiency and payload capacity can be achieved. With sensitively adjusting the lift of the UAV, it is feasible for UAV to quickly change its attitude of motion thus improving the responsiveness of the UAV. Currently, the main methods to change the wing lift are wing optimization and active flow control. In recent years, the use of active flow control technology has become a hot research topic due to its good adaptability.

A synthetic jet actuator, also known as a zero-net-mass-flux actuator, typically consists of a cavity and a piezoelectric membrane that oscillates back and forth around its own equilibrium position and periodically blow/sucks gas. There are privileges that small size, light weight, low power consumption and high sensitivity for it. The local flow field of the wing can be accurately controlled by it without changing the shape of the wing. Synthetic jets are commonly used in airplanes (Zhao).

The research of synthetic jets on wing flow control mainly focuses on aspects such as flow separation control, stall mitigation control, and increasing lift and reducing drag. Seifert studied the mitigation of wing stall phenomenon by synthetic jets. The survey displayed that the airflow separation phenomenon generated on the wing surface could be effectively retarded by using synthetic jets. The retarding effect was related to the position, frequency, and intensity of the synthetic jets. Esmaeili Monir, H., studied the effect of installing synthetic jets along the tangential direction on the aerodynamics of the NACA-23012 wing. It was shown in his study that the lift-to-drag ratio of the wing increased with the increase of the blowing ratio, and when the lift-to-drag ratio reached 3, further increases in the blowing ratio did not affect it. Shmilovich studied a distributed array of synthetic jet flow control schemes on flaps. The results of the study showed that lift could be significantly increased and drag reduced with the distributed array over the range of practical angles of attack. Xu investigated the improvement effect of synthetic jets on the elevation pitching moment of UAV. The research results showed that the larger the momentum coefficient of the jet, the better the control effect on the flow field. When the jet frequency was around 1, the control effect of the vortex interference principle was most significant. Zhou proposed a method of using synthetic jets to prevent airflow separation at the rear end of the wing during aileron deflection. The results showed that the use of synthetic jets could effectively improve the rudder efficiency and lift coefficient by around 20%.

Plasma jet actuator with dielectric barrier discharge type, which is consisted of two electrodes, impart momentum to the fluid under the input of a high AC voltage at high frequency. There are advantages such as no moving parts, small size, fast response and controllability. In recent years, plasma jet actuators have become increasingly popular in the field of flow control (Kolbakir).

Lopera conducted experiments on the control of UAV flight performance by a plasma jet actuator during low angle of attack flight. The results showed that the actuator was able to reattach the separation flow to the airfoil surface, which could effectively improve the lift. Moreau considered the effectiveness of multiple DBD plasma jet actuators in controlling a NACA0015 wing. The results of the study showed that locating the DBD at 18% of the chord length was most effective. Pouryoussefi investigated the effect of installing a DBD plasma jet actuator on the flow control of an iced wing. The results showed that activation of the plasma actuator on an iced wing resulted in a stall angle delay of 2 degrees and a maximum lift coefficient increase of about 6%. Parishani completed flow control experiments on the NACA0024 airfoil using both steady-state and unsteady-state DBD plasma actuators. The results showed that the unsteady actuator produces flow control results was similar to the performance of the steady-state actuator, but the unsteady actuator could significantly reduce the plasma power consumption by approximately 51%. Mazaheri presented a new methodology for simulation of plasma hydrodynamic flow around a DBD actuator installed on an airfoil. The simulation results are in good agreement with the experimental results, which verifies the effectiveness of the method.

Huang investigated the hysteresis phenomenon of lift of pitching airfoil. It is lag effect due to the time required to convect the boundary layer reaction to the pressure gradient change from the leading edge to the point of separation. It is found that continuous changes of the angle of attack in a limited time can cause this lift lag phenomenon. In this paper, similar lift lag phenomena were also observed due to the flow field changes around the wing caused by synthetic jets. The two phenomena are essentially the same, but the reasons for causing boundary layer reactions are different, one is to change the angle of attack, and the other is to increase the control of synthetic jet flow.

In conclusion, the enhancement of wing aerodynamics through flow control has become a popular research focus. However, there are significant differences in the working characteristics between plasma jet actuator and synthetic jet actuator. And their effects on the wing are also different. In this paper, the flow control model used is a plasma actuator and a synthetic jet actuator installed at the leading edge of the aileron. The advantages of the combined flow control mode over a single mode are investigated by means of numerical simulation. And the aerodynamic mechanism of the wing lifting by the combined flow control mode is analyzed. The effects of the plasma voltage, the maximum exit velocity of the synthesized jet, and the deflection angle on the flow control effect are investigated.

2. PHYSICAL MODEL AND NUMERICAL METHODS

2.1 Physical Method

The EPPLER555 wing is the research object of this paper. The wing is composed of the main wing and aileron. Figure 1 shows the schematic diagram of the physical model and jet actuator layout. The flow control method used in this paper is a combination of plasma jet actuator and synthetic jet actuator control. The plasma jet actuator is installed at the Jet_1 position, and the synthesized jet actuator is installed at the Jet_2 position.

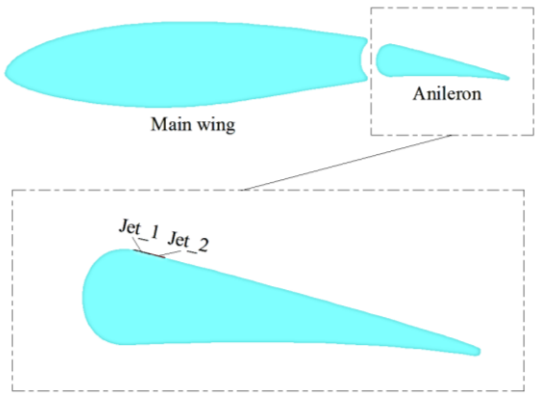

Fig. 1 EPPLER555 model

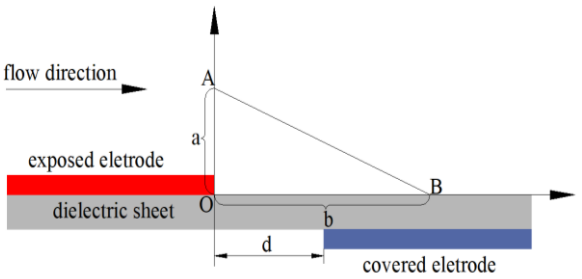

Fig. 2 The model of typical plasma jet actuator

2.2 Numerical Methods

The plasma jet actuators mainly include plasma spark jet actuator and dielectric barrier discharge (DBD) plasma jet actuator, etc. In this paper, the (DBD) plasma actuator is used. In order to improve the computational efficiency, the simulation is carried out by using the phenomenological model of the plasma (Jayaraman). The schematic diagram of the DBD phenomenological model is shown in the following Fig. 2. The line A-B constitutes the plasma fluid boundary using linear approximation. The electric field strength outside this line is not strong enough to ionize the air.

The electric field strength at any point in space can be expressed by the following equation (1).

$$\left|\vec{E}\right| = E_0 - k_1 x - k_2 y \tag{1}$$

$$E_0 = \frac{U}{d} \tag{2}$$

$$k_1 = \frac{E_0 - E_b}{b} \tag{3}$$

$$k_2 = \frac{E_0 - E_b}{a} \tag{4}$$

Where E_0 is the maximum electric field strength, E_b is the boundary voltage, k_1 and k_2 are the gradient of the electric field strength along the x, y direction, and d is the distance between the two electrodes along the x direction.

The component of the electric field is:

$$\begin{cases} E_x = \dfrac{Ek_2}{\sqrt{k_1^2 + k_2^2}} \\ E_y = \dfrac{Ek_1}{\sqrt{k_1^2 + k_2^2}} \end{cases} \tag{5}$$

The volumetric force in the plasma for one discharge duration is：

$$\begin{cases} f_x = \delta E_x \rho_c e_c \\ f_y = \delta E_y \rho_c e_c \end{cases} \tag{6}$$

Where ρ_c is the charge density and e_c is the electronic charge.

Hence the force can be time-averaged over a complete cycle although it exists only for a small time per cycle:

$$\begin{cases} F_x = \dfrac{f_x \Delta t}{T} \\ F_y = \dfrac{f_y \Delta t}{T} \end{cases} \tag{7}$$

Where T is the plasma discharge period.

Since plasma-induced jets are operated at low Reynolds numbers and are essentially isothermal phenomena, the fluid is assumed to be incompressible. The 2D state control equations are the following.

$$\frac{\partial}{\partial t}\begin{bmatrix} \rho \\ \rho u \\ \rho v \end{bmatrix} + \frac{\partial}{\partial x}\begin{bmatrix} \rho u \\ \rho u^2 + p - \tau_{xx} \\ \rho uv - \tau_{xy} \end{bmatrix} + \frac{\partial}{\partial y}\begin{bmatrix} \rho v \\ \rho uv - \tau_{xy} \\ \rho v^2 + p - \tau_{xy} \end{bmatrix} = \begin{bmatrix} 0 \\ F_x \\ F_y \end{bmatrix} \tag{8}$$

Where F_x, F_y are the body forces, is the shear stress.

The effect of the synthetic jet actuator is described by velocity inlet boundary. The exit velocity of the synthetic jet is a sinusoidal function, as shown in the following equation.

$$V_{SJA} = V_{\max} \sin(\omega t + \varphi) \tag{9}$$

Where V_{max} is the maximum exit velocity of the synthetic jet actuator, ω is the frequency, and φ is the initial stage angle.

3. ACCURACY VERIFICATION AND GRID INDEPENDENCY TEST

3.1 Accuracy Verification

In this paper, the solution of the compressible Navier-Stokes equation is obtained using a commercial solver Fluent 2022. The Standard k-ω model is used in the modeling in this stage. The pressure-based solution is used in the solution methods. The second-order windward method is used about the spatial discretization. The time step is 0.001s, the maximum iteration of each time step is 20, and the computation time is 1s. In order to verify the accuracy of the numerical method adopted, the experimental results in the literature are used to verify the solution method adopted in this paper, and the boundary conditions are consistent with those in the literature (Hasegawa). The calculation model is shown in Fig. 3(a). The NACA0012 airfoil had a chord of 200 mm, the freestream velocity is 10m/s, and the corresponding Reynolds number is 1.5×10^5. Figure 3(b) shows that when using the NACA0012 airfoil in the literature, the lift coefficients at different angles of attack are well combined, and the difference may come from a two-dimensional assumption.

The accuracy of the plasma jet actuator simulation model was validated with W.Shyy's flat plate model (Shyy). The calculation model is shown in Fig. 4(a). The high of electrode is 0.1mm, the freestream velocity is 5m/s, and the corresponding Reynolds number is 34.2. The velocity distribution curve at 3.8mm behind the plasma

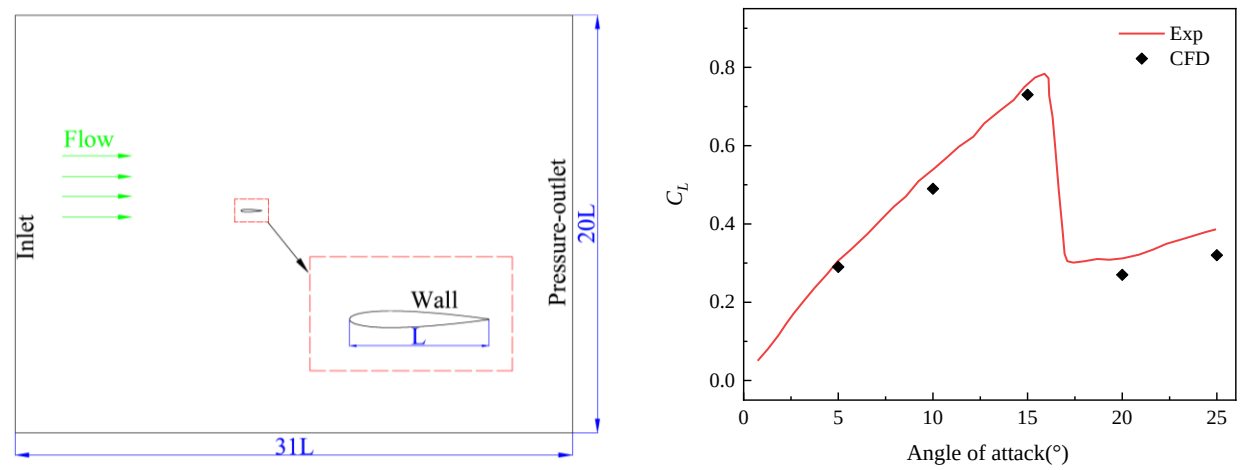

(a) Computation model (b) Variation of lift coefficients with angle of attack

Fig. 3 Calculation model and lift coefficient curve

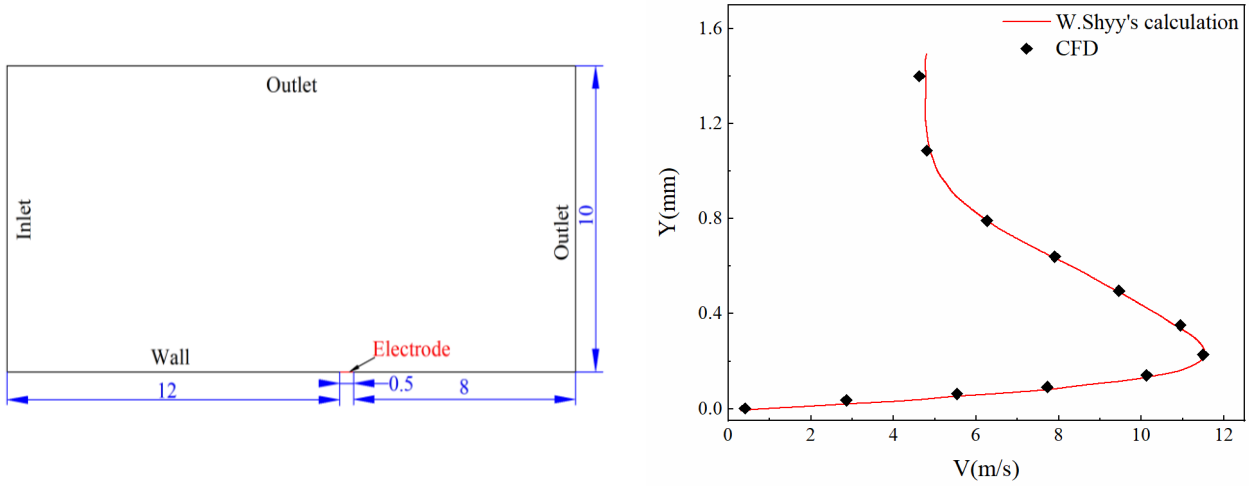

(a) Computation model (b) Velocity distribution in the Y direction

Fig. 4 Calculation model and velocity distribution curve

jet actuator is shown in Fig. 4(b). The calculation results in this paper are basically consistent with W. Shyy's results. Thus, it can be considered that the plasma simulation method used in this paper is accurate.

3.2 Grid Independency Test

The mesh is shown in Fig. 5. The chord length of the wing is L, the flow field is a rectangular flow field with a length of 31L and a height of 20L. The width of actuators is 0.01L.

The inlet boundary is the velocity inlet, the incoming velocity is 20m/s, the wall of main wing and aileron are set as adiabatic boundary condition and stationary no-slip wall. The effect of the plasma actuator is simulated by the momentum source term, and the synthetic jet actuator is simulated by the velocity inlet. The structured mesh is used in the paper. To ensure accurate aerodynamic calculations, the height of the first layer of the grid should be set to 0.01mm. The mesh independence is achieved by three levels of mesh refinement. The lift coefficients for different grid numbers are shown in Fig. 6. There is very little difference between the medium and maximum number grids. Therefore, mesh of 126,753 is chosen for simulation to ensure calculation accuracy and reduce calculation time.

4. CONTROL EFFICIENCY ANALYSIS

4.1 Comparison of Different Flow Control Modes

First, the aerodynamic results of the wing under different flow control modes are analyzed. The flow control modes are shown in Table 1. The flow control

Table 1 Flow control modes

Mode	Jet_1	Jet_2
No control	—	—
PJA control	plasma jet actuator	—
SJA control	—	synthetic jet actuator
PAS control	plasma jet actuator	synthetic jet actuator
SAP control	synthetic jet actuator	plasma jet actuator

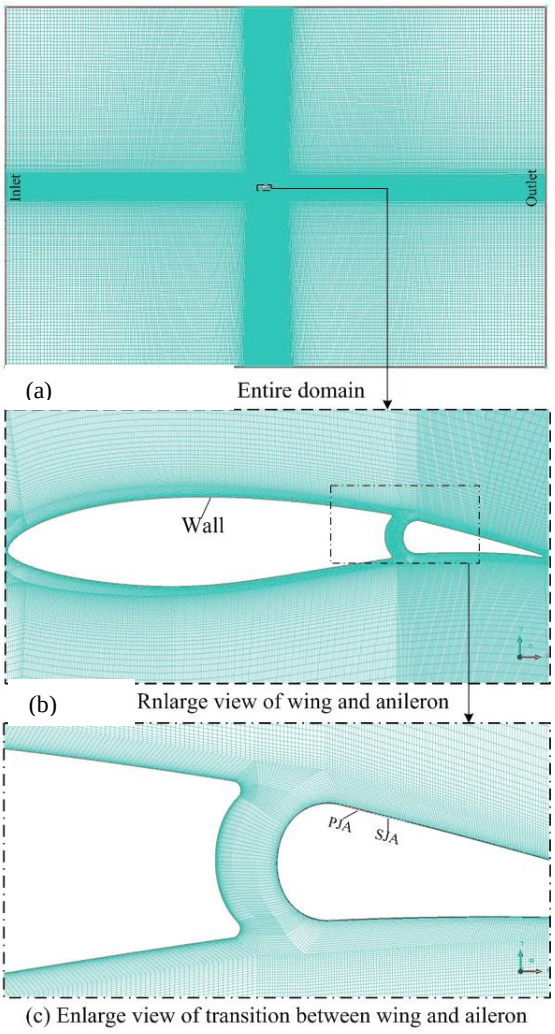

Fig. 5 Mesh distribution

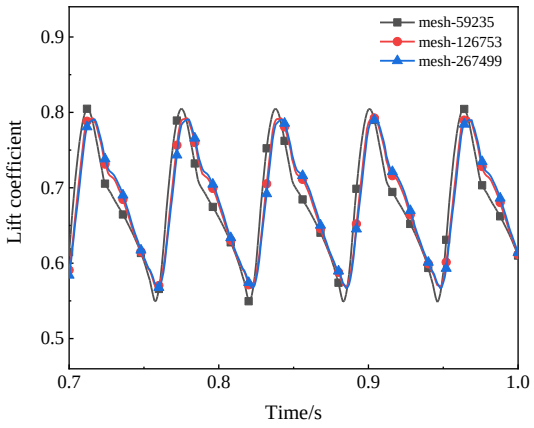

Fig. 6 Variation of lift coefficient with mesh size and time

modes： 1) No control; 2) Single plasma jet actuator (PJA) control; 3) Single synthetic jet actuator (SJA) control; 4) Combination mode of plasma jet actuator installed before synthesis jet actuator (PAS); 5) Combination mode of synthesis jet actuator installed before plasma jet actuator (SAP).

Figure 7 shows the wing pressure cloud and the vorticity magnitude cloud at t=0.9s for various flow control modes. The pressure cloud displays that the negative pressure area on the upper surface of the aileron is significantly increased by the flow control. The effect of the jet disturbance extends from the aileron to the main wing, which means that the installation of an actuator above the aileron could have a beneficial effect on the main wing.

In order to further characterize the wing surface pressure distribution, Fig. 8 and Fig. 9 show the pressure distribution curves on the main wing and aileron surfaces with different flow control modes. As shown in Fig. 8, when flow control devices are installed, the upper surface pressure of the main wing decreases. Consequently, the lower surface pressure increases, and the pressure difference between the upper and lower surfaces of the main wing increases significantly. The pressure difference in the combined flow control mode is significantly greater than in the single flow control mode. The pressure distributions on the main wing surface are almost the same in the combined PAS and SAP flow control modes. Only at the trailing edge of the main wing, the pressure difference in PAS control mode is slightly larger than that in SAP control mode. As shown in Fig. 8, the pressure difference between the upper and lower surfaces of the aileron in the combined control mode is higher than that in the single control mode. And the pressure fluctuation of PAS mode is smaller than that of SAP near the actuator in the combined control mode.

Figure 10 shows the variation of the wing lift coefficient with time for different control modes. The lift coefficient curve of the wing under uncontrolled and single plasma jet actuator control are straight and stable. The lift curves of the single synthetic jet actuator control and the combined mode control show periodic fluctuations. The the fluctuation period is corresponded to the working period of the synthetic jet. It is obvious that the lift coefficient increase is most effective when the PAS control mode is used. Therefore, the effects of the flow field and related control parameters under PAS flow control mode will be discussed in detail.

4.2 Flow Field Analysis

Due to the periodic fluctuation of the lift coefficient of the wing after the addition of PAS flow control, the flow field within one cycled is analyzed in detail in this section. The plasma voltage is 50kV, and the max exit velocity of the synthetic jet is 90m/s. During 1/16T-8/16T, the synthetic jet actuator is in "blowing" stage. During the 9/16T-16/16T time period, the synthetic jet actuator is in the "suck" stage.

From Fig. 11, it can be seen that the flow field vorticity magnitude increases and then decreases, which corresponds to working characteristics of the synthetic jet. In the "blowing" stage, the vorticity magnitude on the aileron upper surface increases. In the "sucking" stage, the vorticity magnitude on the aileron upper surface decreases. The vorticity magnitude near the plasma jet actuator is always higher.

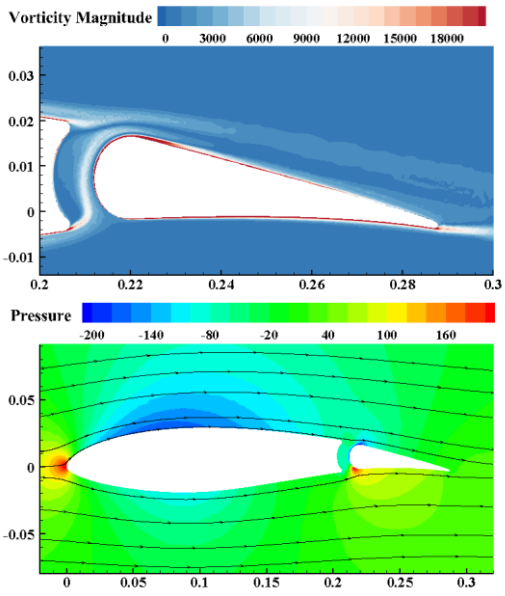

(a) No-control

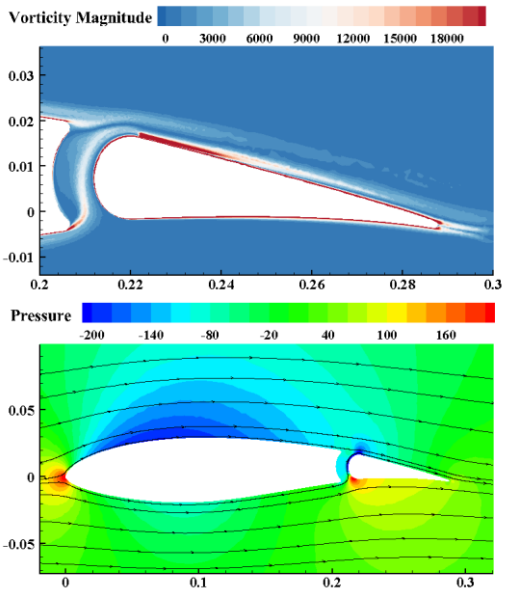

(b) PJA-Control

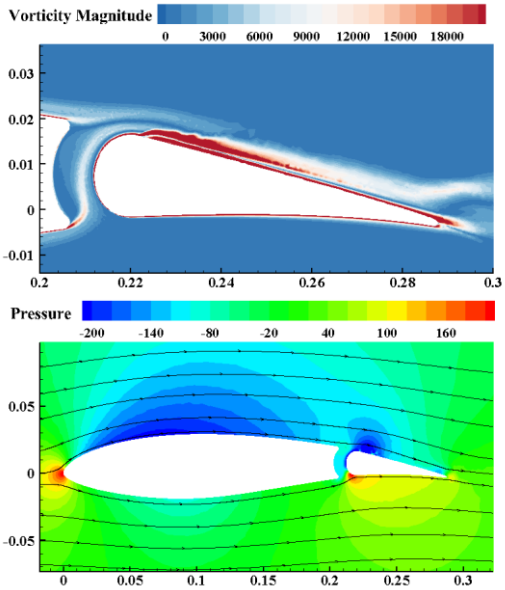

(c) SJA-Control

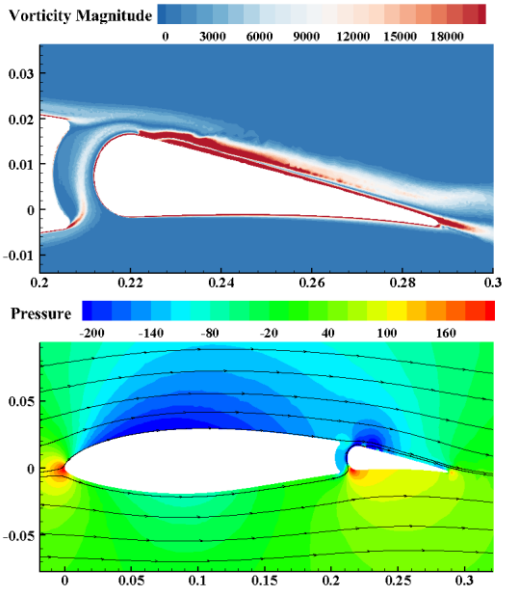

(d) PAS-Control

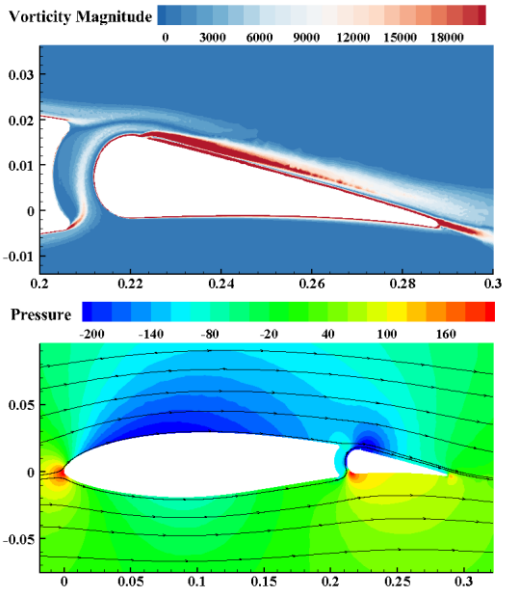

(e) SAP-Control

Fig. 7 Flow field comparison of pressure and vorticity magnitude with different control mode

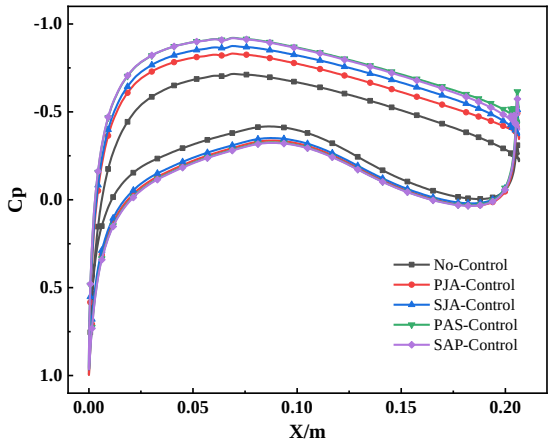

Fig. 8 Comparison of pressure coefficient of main wing with different control mode

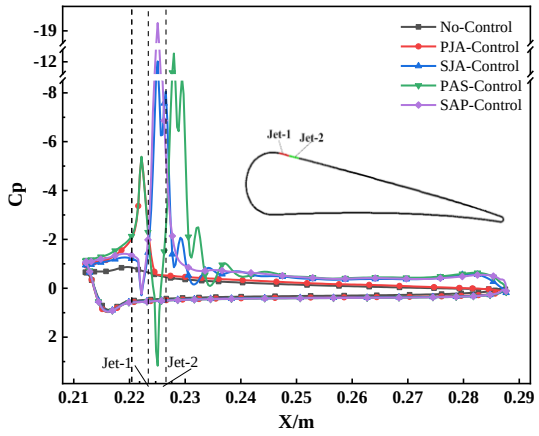

Fig. 9 Comparison of pressure coefficient of aileron with different control mode

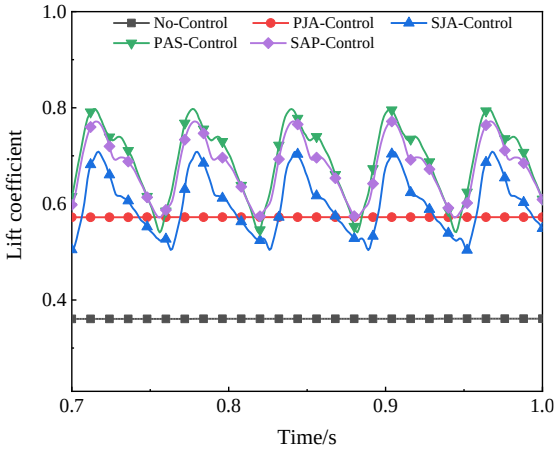

Fig. 10 Variation of lift coefficient with control mode

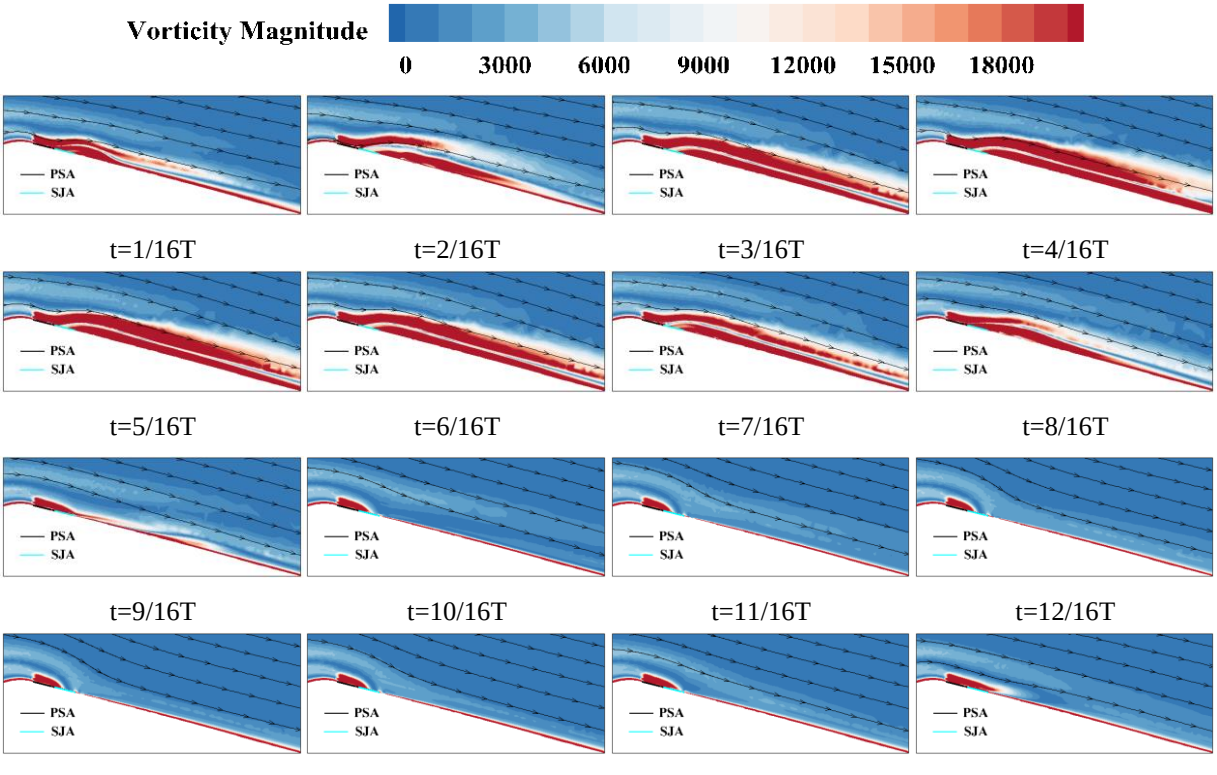

Fig. 11 Variation of vorticity magnitude superposed streamlines on aileron

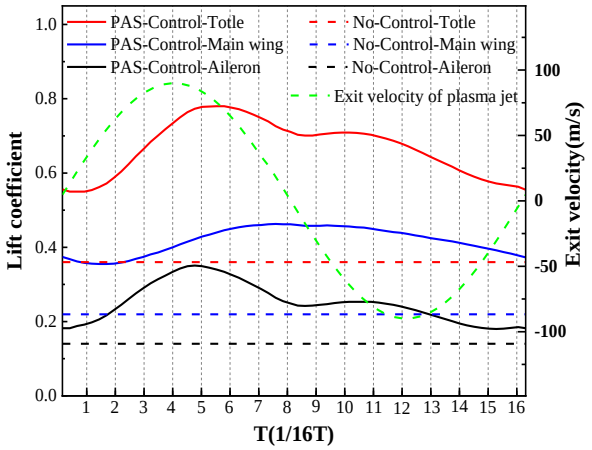

Fig. 12 Variation of lift coefficient of wing and aileron and exit velocity of PAS with time

The lift of the wing is the sum of the main wing lift and the aileron lift. Figure 12 shows the variation of the lift coefficient for PSA control mode and uncontrolled mode during a single cycle. In the "blowing" stage, it can be seen from Fig. 12 that the lift coefficient of the aileron increases first and then decreases over time. The peak lift coefficient of ailerons occurs between 4/16T-5/16T, and the moment of the peak lift coefficient of ailerons is the same as the moment of the peak "blowing" of the synthetic jet. This indicates that when the surface airflow velocity on the aileron reaches its maximum, the lift enhancement effect of the aileron is the best, and the vorticity near the aileron also reaches its maximum. The lift coefficient of the main wing also increases significantly, and the peak lift coefficient of the main wing occurs between 8/16T-9/16T, which delayed behind the peak lift coefficient of the aileron. The phenomenon of delay is explained in Fig. 13. From the graph, it can be seen that there is a low-pressure area on the upper surface of the aileron, which first expands and then shrinks, resulting in an increase and then a decrease in the lift coefficient of the aileron. At the same time, the low-pressure area on the surface of the aileron will have a traction effect on the high-pressure area above the main wing, causing airflow acceleration and pressure reduction above the main wing. And this process is relatively slow, which leads to a lag in the peak lift of the main wing.

In the "suction" stage, the synthetic jet actuator begins sucking back air. As the suction speed increases, the lift coefficient of the aileron first shows a slight upward trend and then decreases. At the same time, the traction effect of the low-pressure area on the upper surface of the aileron on the airflow above the main wing gradually decreases. The pressure above the main wing begins to increase, and the lift coefficient of the main wing begins to gradually decrease.

In order to describe the contribution of the lift increase within the main wing and the aileron, the lift coefficient increase percentage is defined, as shown in the following equation:

$$C_{l\_increase\_i} = \frac{C_{l\_PAS\_i} - C_{l\_No\_i}}{C_{l\_PAS\_Total} - C_{l\_No\_Total}} \quad (10)$$

$$i = Wing, Anileron$$

Where $C_{l\_PSA\_i}$ is the wing or aileron lift coefficient in PAS mode, $C_{l\_No\_i}$ is the wing or aileron lift coefficient in no control mode, $C_{l\_PAS\_Total}$ are the total lift coefficient in PAS mode, and $C_{l\_No\_Total}$ is the total lift coefficient in no control mode.

Figure 14 demonstrates the variation of the percentage of aileron lift and main wing lift over a period of time. In general, the main wing lift increase percentage are greater than the aileron lift increase percentage. When the exit velocity of synthetic jet actuator is 0, the maximum of main wing lift increase percentage is 79%, and the aileron lift gain percentage is only 21%. Only between 3/16T-5/16T, the aileron lift increase percentage is slightly higher than the main wing lift increase percentage.

5. STUDY ON EFFECTS OF FLOW CONTROL PARAMETERS

Although it has been proved in the content above that the PAS flow control mode can effectively improve the wing lift coefficient, but the control effects greatly depend on the selection of flow control parameters. Therefore, it is necessary to analyze the role of typical flow control parameters on control efficiency.

5.1 Effect of Maximum Exit Velocity of Synthetic Jet

In this section, five cases are set in comparison, with maximum exit velocity of synthetic jet about 50m/s, 60m/s, 70m/s, 80m/s and 90m/s. As shown in Table 2, it can be seen that as the maximum exit velocity of the synthetic jet increases, the maximum lift coefficient increases significantly from 0.613 to 0.791. At the same time, the fluctuation amplitude of the lift coefficient increases correspondingly from 0.141 to 0.223. The main reason is that as the maximum exit velocity of the synthetic jet increases, the "blowing" and "sucking" processes of the synthetic jet become more intense, causing an increase in the amplitude of the lift fluctuations. Figure 15 and Fig. 16 shows that the average lift coefficient increases as the maximum exit velocity of the synthetic jet increases, and the average lift coefficient increase is from 56% to 86.7%, when the exit velocity of the synthetic jet is increased from 50m/s to 90m/s.

Table 2 Parameter comparison of PAS with different exit velocity

Maximum exit velocity(m/s)	Voltage(kV)	Cl_{max}	Cl_{max}-Cl_{min}
50	50	0.613	0.141
60	50	0.653	0.161
70	50	0.698	0.182
80	50	0.744	0.201
90	50	0.791	0.223

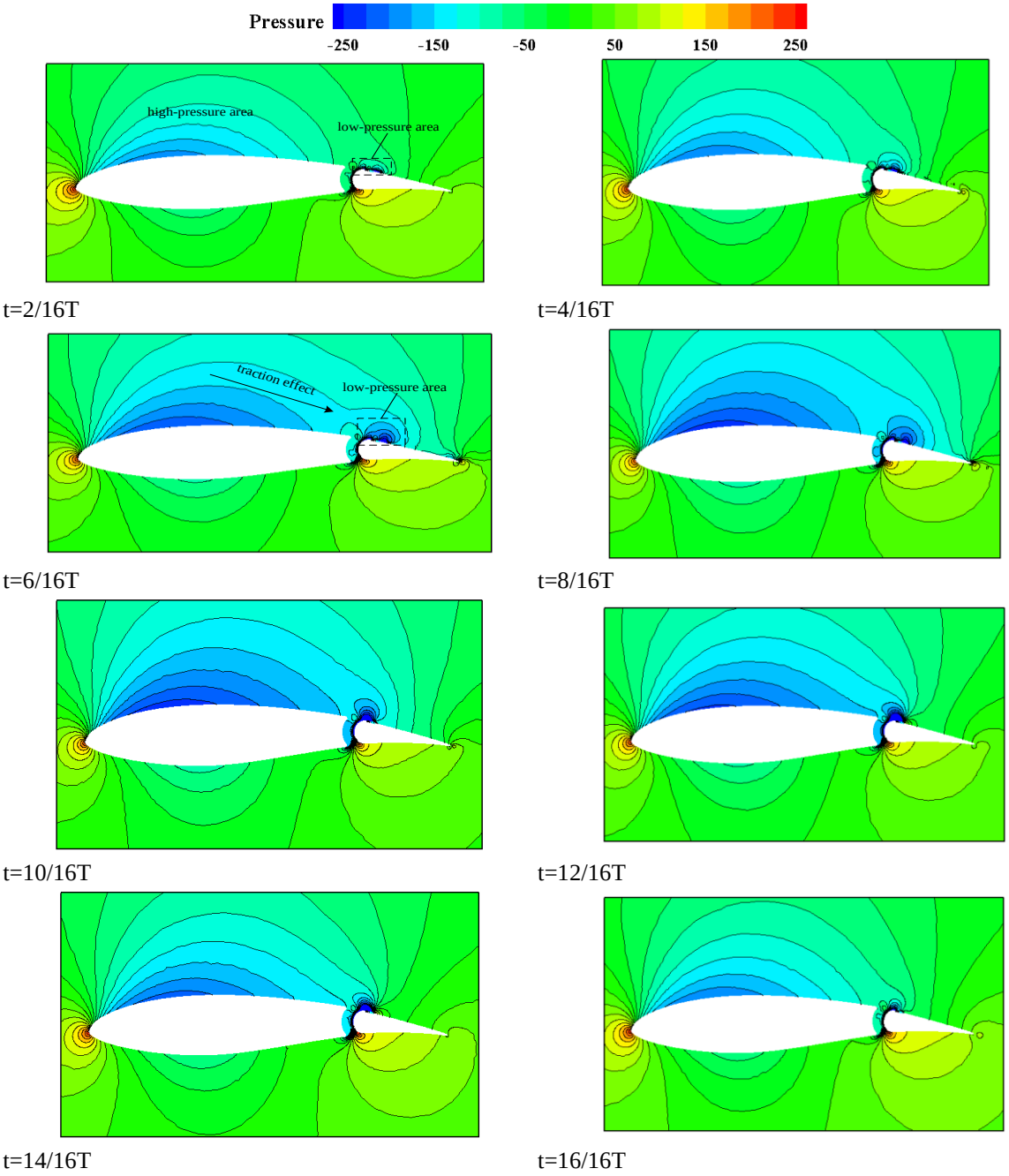

Fig. 13 Variation of pressure of main wing and aileron with time

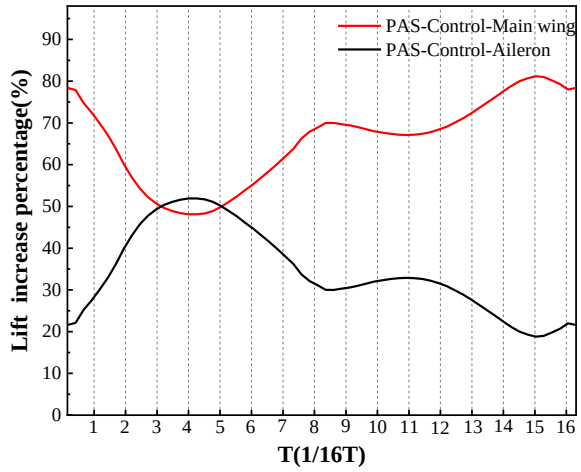

Fig. 14 Variation of lift coefficient increase about wing and aileron

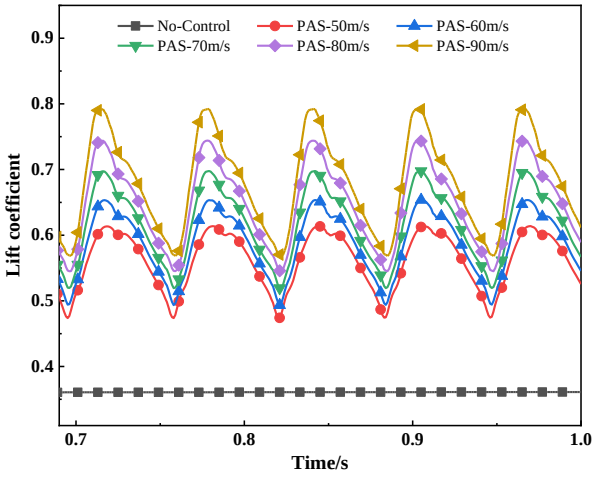

Fig. 15 Variation of lift coefficient with maximum exit velocity

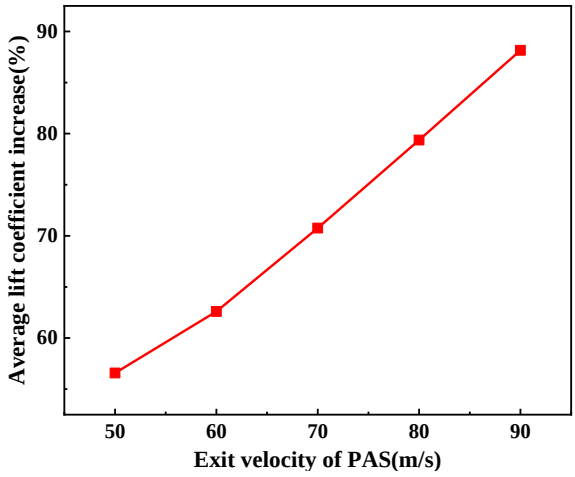

Fig. 16 Variation of lift coefficient increase with maximum exit velocity

Figure 17 shows the typical vorticity magnitude field under different maximum exit velocity when t=0.9s. The vorticity magnitude on the upper surface of the aileron can be used as one of the bases for judging the effectiveness of the wing lift increase. The greater the vorticity magnitude generated by the actuators, the higher the effect of improving wing lift. It can be seen that as the maximum exit velocity increases, the aileron upper surface vorticity magnitude becomes more powerful and the aileron trailing edge vorticity area becomes larger.

5.2 Effect of Plasma Voltage

In this section, five cases are set in comparison, with voltage of plasma jet actuator of 10kV, 20kV, 30kV, 40kV and 50kV. And the maximum exit velocity of the synthetic jet actuator is 90m/s. As shown in Table 3, while the plasma discharge voltage increases, the maximum lift coefficient increases and the lift coefficient amplitude increases slightly. As shown in Fig. 18 and Fig. 19, the change of the plasma voltage has less effect on the fluctuation of the lift coefficient curves. Increasing the plasma voltage can stably improves the lift coefficient of the wing. When the discharge voltage increases from 10kV to 50kV, the average lift coefficient increases linearly from 76.5% to 86.7%.

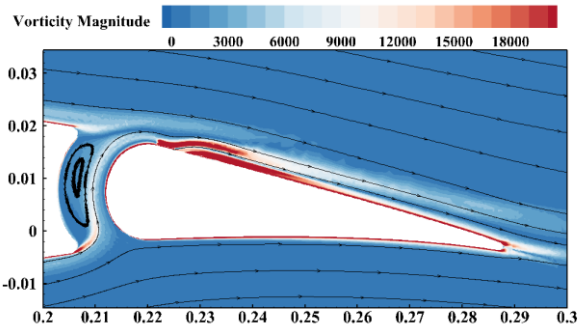

(a) V_{max}=50m/s, U=50kV

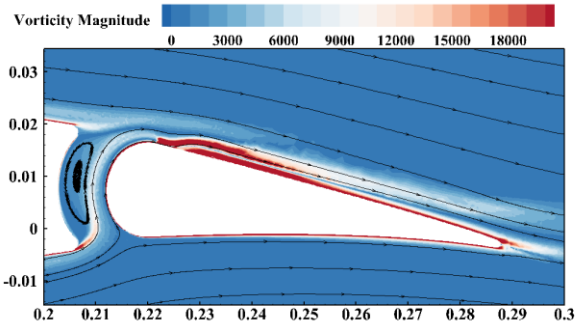

(b) V_{max}=60m/s, U=50kV

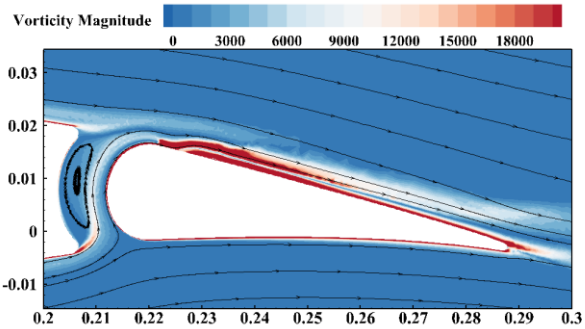

(c) V_{max}=70m/s, U=50kV

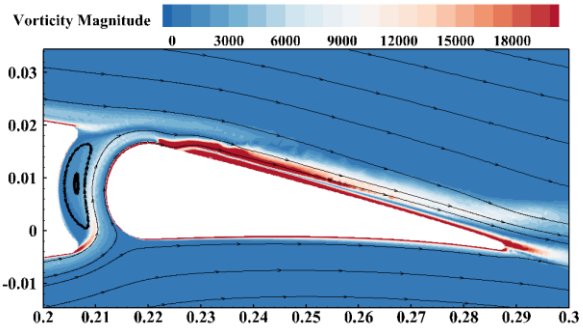

(d) V_{max}=80m/s, U=50kV

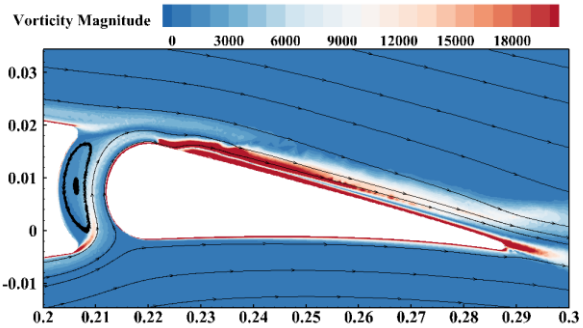

(e) V_{max}=90m/s, U=50kV

Fig. 17 Variation of vorticity with different maximum exit velocity

Table 3 Parameter comparison of PAS with different voltage

Voltage(kV)	Maximum exit velocity(m/s)	Cl_{max}	Cl_{max}-Cl_{min}
10	90	0.738	0.213
20	90	0.752	0.214
30	90	0.767	0.216
40	90	0.779	0.219
50	90	0.792	0.223

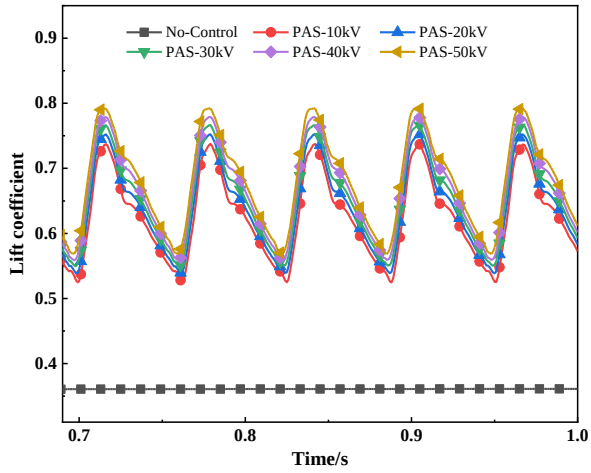

Fig. 18 Variation of lift coefficient with voltage

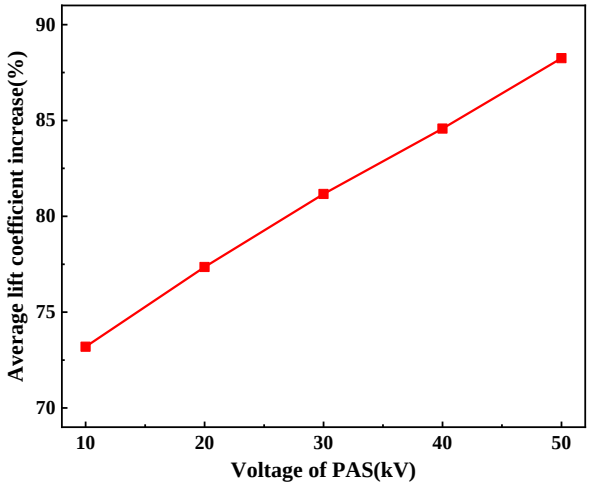

Fig. 19 Variation of lift coefficient increase with voltage

Figure 20 describes the typical vorticity magnitude field under different voltages when t=0.9s. It can be seen that the vorticity magnitude in the plasma discharge region increases significantly with increasing plasma voltage, but the vorticity magnitude of aileron increase is small. The reason is that the energy injected into the boundary layer of the aileron by the synthetic jet blowing is much greater than that injected by the plasma jet at this moment, and the vorticity on the surface of the entire aileron is mainly generated by the synthetic jet.

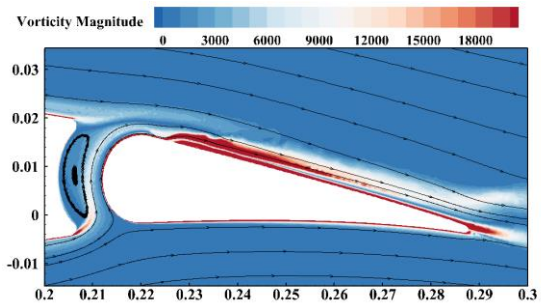

(a) V_{max}=90m/s, U=10kV

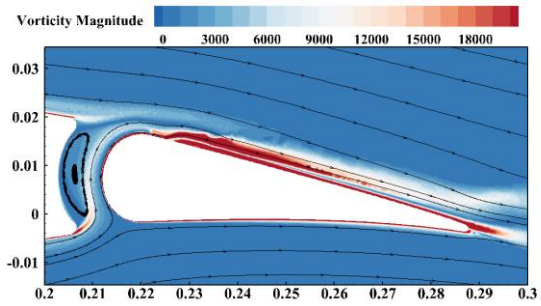

(b) V_{max}=90m/s, U=20kV

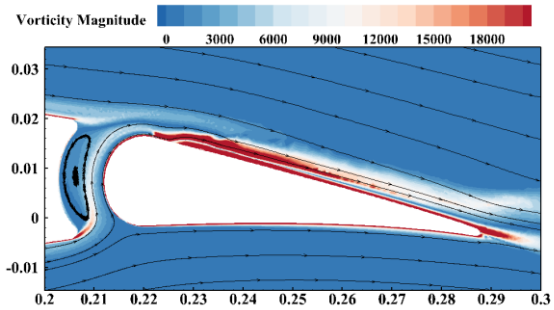

(c) V_{max}=90m/s, U=30kV

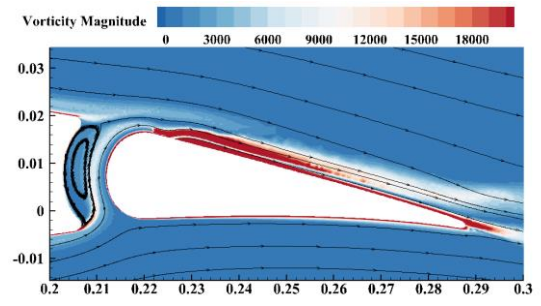

(d) V_{max}=90m/s, U=40kV

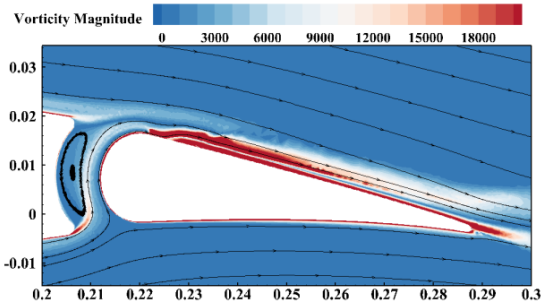

(e) V_{max}=90m/s, U=50kV

Fig. 20 Variation of vorticity with different voltage

Table 4 Parameter comparison of PAS with different voltage and exit velocity

Voltage(kV)	Maximum exit velocity(m/s)	Cl_{max}	Cl_{max}-Cl_{min}
10	50	0.533	0.105
20	60	0.603	0.138
30	70	0.668	0.167
40	80	0.731	0.195
50	90	0.792	0.223

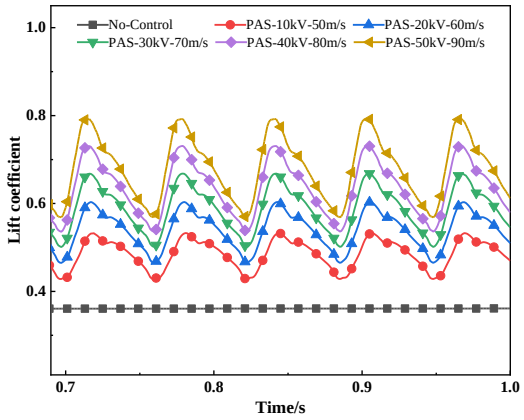

Fig. 21 Variation of lift coefficient with voltage and exit velocity

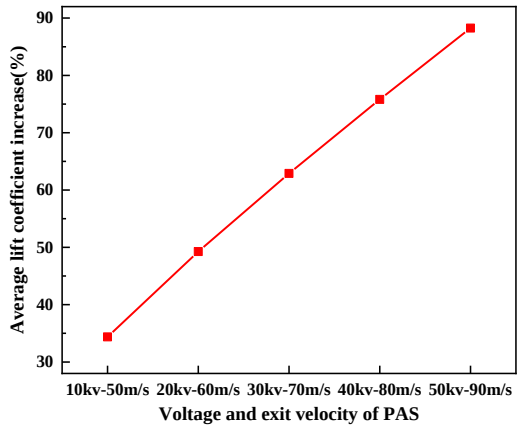

Fig. 22 Variation of lift coefficient increase with voltage and exit velocity

5.3 The Effect of Simultaneous Changes in Voltage and Velocity

In this section, plasma voltage and synthetic jet exit velocity are varied simultaneously and five operating conditions are compared as shown in Table 4. It can be seen that the maximum lift coefficient increases from 0.533 to 0.792. The the amplitude of the maximum lift coefficient fluctuation increases from 0.105 to 0.223 with the increase of the synthetic jet exit velocity and plasma discharge voltage. As shown in Fig. 21 and Fig. 22, changing both the plasma voltage and the maximum exit velocity of the synthetic jet had a significant effect on the lift coefficient profile, with the average lift coefficient improvement increasing from 34% to 86.7%.

Figure 23 shows the typical vorticity magnitude field under different voltages and exit velocity when t=0.9s. It is shown that as plasma voltage and synthetic jet exit velocity are increased, the vorticity magnitude of aileron surface and trailing edge of aileron increases significantly.

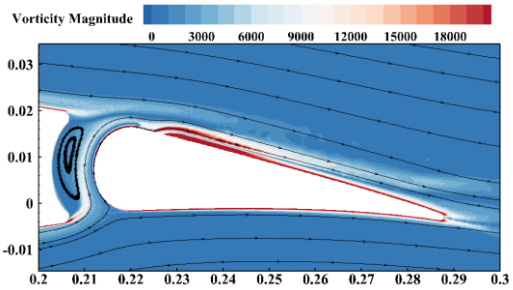

(a) V_{max}=50m/s,U=10kV

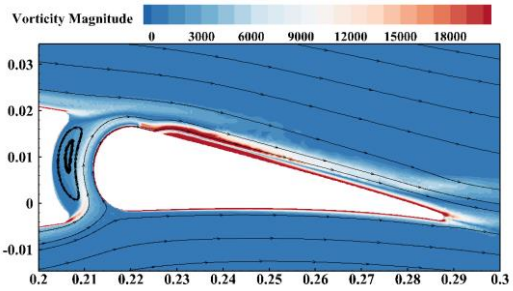

(b) V_{max}=60m/s, U=20kV

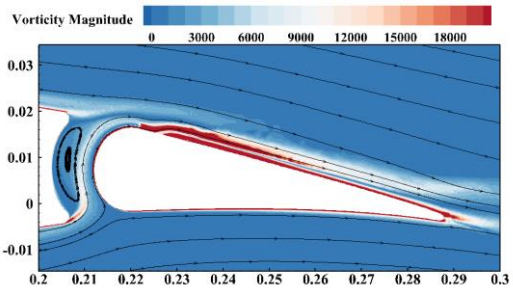

(c) V_{max}=70m/s, U=30kV

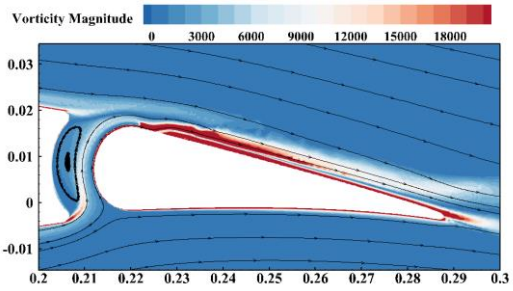

(d) V_{max}=80m/s, U=40kV

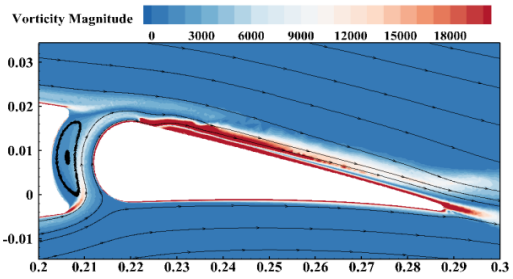

(e) V_{max}=90m/s, U=50kV

Fig. 23 Variation of vorticity with different maximum exit velocity and voltage

Table 5 Parameter comparison of aileron with different deflection angle

Angle (°)	Voltage (kV)	Maximum exit velocity(m/s)	Cl_{max}	Cl_{max}-Cl_{min}
4	50	90	0.792	0.223
5	50	90	0.860	0.232
6	50	90	0.934	0.245
7	50	90	1.010	0.258
8	50	90	1.080	0.276

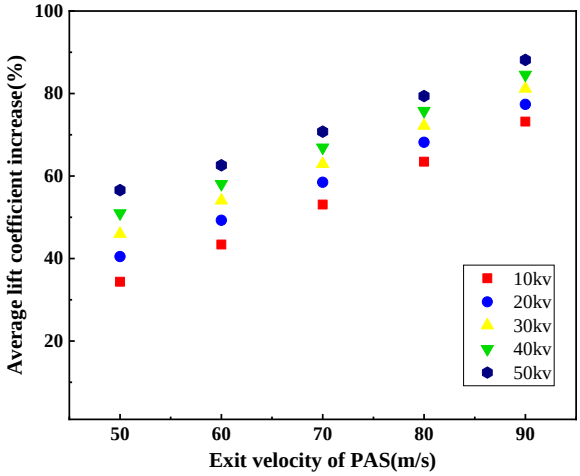

Fig. 24 Variation of lift coefficient increase with voltage and maximum exit velocity

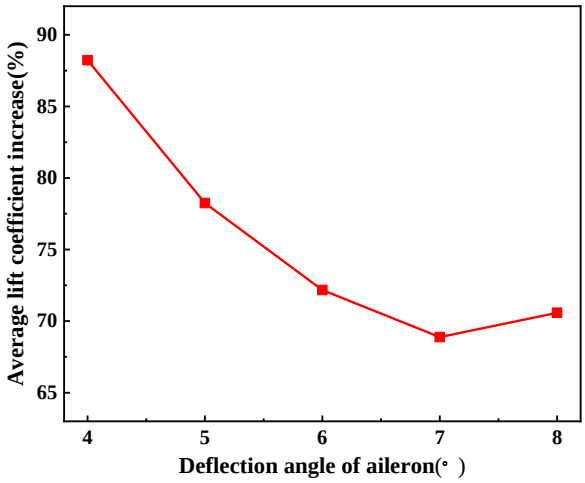

Fig. 26 Variation of average lift coefficient increase with aileron deflection angle

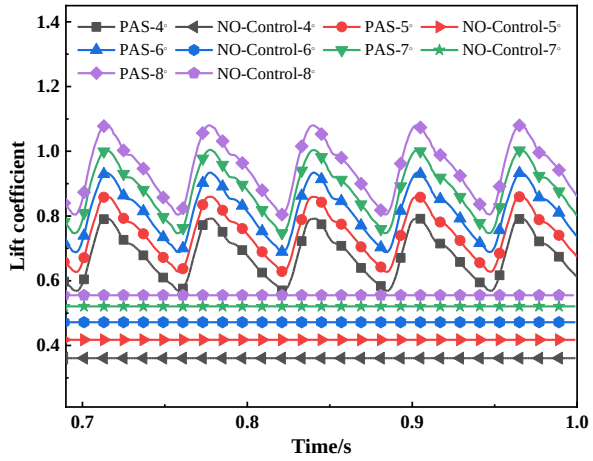

Fig. 25 Variation of lift coefficient with aileron deflection angle

In order to provide a more comprehensive description of the effects with plasma voltage and synthetic jet exit velocity on lift, Fig. 24 shows the variation of average lift coefficient increase under different plasma voltages and exit velocity. When the exit velocity of the synthetic jet is smaller, the effect of the plasma voltage change on the lift rate is greater. For instance, when exit velocity is 50m/s, increasing the voltage from 10kV to 50kV results in a lift rate increase from 34.3% to 56.6%, which is a 22.3% increase. When exit velocity is 90m/s, increasing the voltage from 10kV to 50kV result in an increase in lift enhancement rate from 73.1% to 88.2%, a difference of only 15.1%.

5.4 Effect of Rudder Deflection Angle

In this section, the effect of the PAS flow control mode is investigated for different rudder deflection angles. Five cases are set in comparison, with deflection angles of 4°, 5°, 6°, 7° and 8°. From Table 5, it can be seen that as the rudder deflection angle increases, the maximum value of the lift coefficient increases and the amplitude of the lift coefficient increases. Figure 25 shows that the installation of PAS flow control devices results in a significant increase in lift coefficient for various rudder deflection conditions. Figure 26 shows that the average lift coefficient increases and then decreases with the deflection angle increases. When the rudder deviation angle is 7°, the increase of average lift coefficient is the lowest. Figure 27 shows that the vorticity magnitude of the aileron surface increases as the deflection angle increases for the same flow control parameters.

6. CONCLUSIONS

In this paper, the mechanism of enhancing the lift of fixed-wing UAVs by plasma jet actuator and synthetic jet actuator is investigated. The effects of plasma voltage, maximum exit velocity of synthetic jet and rudder deflection angle on the control effect are analyzed in detail. The main conclusions are as follows:

(1) The use of PAS flow control mode can greatly improve the wing lift. Installing the flow control device on the aileron can simultaneously increase the lift of both the aileron and the main wing, with a more significant increase in the lift of the main wing. The low-pressure area generated by the flow control device will pull and accelerate

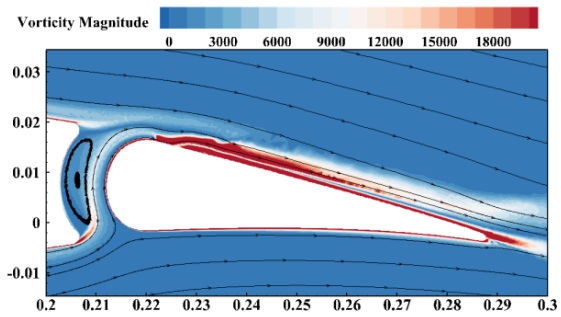

(a) 4° deflection angle

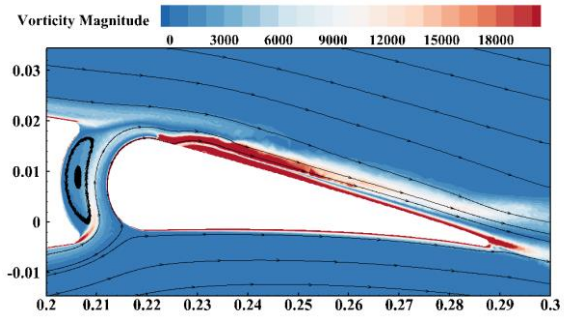

(b) 5° deflection angle

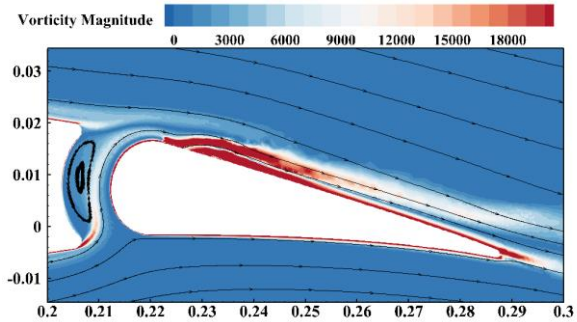

(c) 6° deflection angle

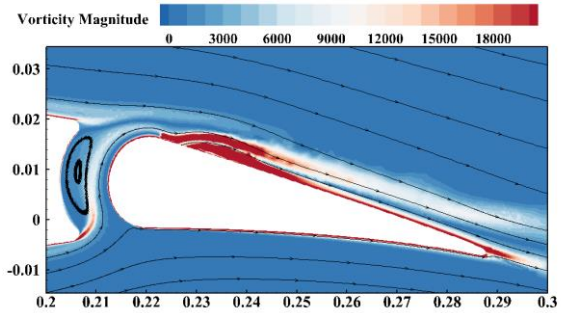

(d) 7° deflection angle

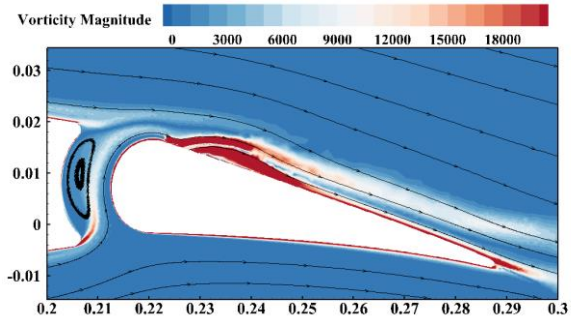

(e) 8° deflection angle

Fig. 27 Variation of vorticity magnitude with aileron deflection angle

the airflow above the main wing, causing a decrease in surface pressure on the lift of the main wing. The sustained traction effect of the low-pressure area on the airflow above the main wing is the main reason for the increase in wing lift.

(2) The periodic disturbance generated by the synthetic jet enhances the turbulent energy of the aileron boundary layer and accelerates the flow velocity of the aileron boundary layer, thereby causing an increase in the intensity of surface vorticity on the aileron. This effect can be further enhanced by installing a plasma jet actuator at the front of the synthetic jet actuator.

(3) When using the PAS flow control mode, increasing the plasma voltage can steadily increase the wing lift, whereas increasing the synthetic jet synthetic jet exit velocity can also cause increased lift fluctuations while increasing the lift. The effect on wing lift caused by changing the plasma voltage is reduced as the synthetic jet exit velocity increases. Therefore, selecting the appropriate maximum exit velocity of the synthetic jet can better regulate the plasma voltage. Additionally, as the angle of deflection increases, the lift enhancement effect produced by the flow control method decreases. This effect is at its lowest when the angle is 7°, with a slight recovery at 8°.

CONFLICT OF INTEREST

The authors declare no conflict of interest.

AUTHORS CONTRIBUTION

Ning Ding: Writing original draft; **Fei Gao**: Validation; **Changjun Tang**: Investigation; **Jianlong Chang**: Project administration.

REFERENCES

Elmeseiry, N., Alshaer, N., & Ismail, T. (2021). A detailed survey and future directions of unmanned aerial vehicles (UAVs) with potential applications. *Aerospace*, *8*(12). https://doi.org/10.3390/aerospace8120363

Esmaeili Monir, H., Tadjfar, M., & Bakhtian, A. (2014). Tangential synthetic jets for separation control. *Journal of Fluids and Structures*, *45*, 50-65. https://doi.org/10.1016/j.jfluidstructs.2013.11.011

Hasegawa, H., & Obayashi, S. (2019). Active stall control system on naca0012 by using synthetic jet actuator. *Journal of Flow Control, Measurement & Visualization*, *07*(01), 61-72. https://doi.org/10.4236/jfcmv.2019.71005

Huang, C., Zhao, L., Niu, J. P., Di, J. J., Yuan, J. J., Zhao, Q. L., Zhang, F. Q., Zhang, Z. H., Lei, J. M., & He, G. P. (2022). Coupled particle and mesh method in an Euler frame for unsteady flows around the pitching airfoil. *Engineering Analysis with Boundary Elements*, *138*, 159-176. https://doi.org/10.1016/j.enganabound.2022.02.011

Jayaraman, B., & Shyy, W. (2008). Modeling of dielectric barrier discharge-induced fluid dynamics and heat transfer. *Progress in Aerospace Sciences*, *44*(3), 139-191. https://doi.org/10.1016/j.paerosci.2007.10.004

Kolbakir, C., Hu, H., Liu, Y., & Hu, H. (2020). An experimental study on different plasma actuator layouts for aircraft icing mitigation. *Aerospace Science and Technology*, *107*. https://doi.org/10.1016/j.ast.2020.106325

Lopera, J., Ng, T. T., Patel, M. P., Vasudevan, S., Santavicca, E., & Corke, T. C. (2007). Aerodynamic control of using windward-surface plasma actuators on a separation ramp. *Journal of Aircraft*, *44*(6), 1889-1895. https://arc.aiaa.org/doi/10.2514/1.30741

Mazaheri, K., Omidi, J., & Kiani, K. C. (2016). Simulation of DBD plasma actuator effect on aerodynamic performance improvement using a modified phenomenological model. *Computers & Fluids*, *140*, 371-384. https://doi.org/10.1016/j.compfluid.2016.10.015

McEnroe, P., Wang, S., & Liyanage, M. (2022). A survey on the convergence of edge computing and ai for uavs: opportunities and challenges. *IEEE Internet of Things Journal*, *9*(17), 15435-15459. https://doi.org/10.1109/jiot.2022.3176400

Moreau, E., Debien, A., Breux, J. M., & Benard, N. (2016). Control of a turbulent flow separated at mid-chord along an airfoil with DBD plasma actuators. *Journal of Electrostatics*, *83*, 78-87. https://doi.org/10.1016/j.elstat.2016.08.005

Parishani, H. (2016). Experimental investigation of separation control on a NACA0024 Airfoil using stationary and non-stationary AC-Dielectric barrier discharge plasma actuator. *Journal of Applied Fluid Mechanics*, *9*(2), 877-888. https://doi.org/10.18869/acadpub.jafm.68.225.24432

Pouryoussefi, S. G., Mirzaei, M., Alinejad, F., & Pouryoussefi, S. M. (2016). Experimental investigation of separation bubble control on an iced airfoil using plasma actuator. *Applied Thermal Engineering*, *100*, 1334-1341. https://doi.org/10.1016/j.applthermaleng.2016.02.133

Seifert, A., Darabi, A., & Wyganski, I. (1996). Delay of airfoil stall by periodic excitation. *Journal of Aircraft*, *33*(4), 691-698. https://arc.aiaa.org/doi/10.2514/3.47003

Shakhatreh, H., Sawalmeh, A. H., Al-Fuqaha, A., Dou, Z., Almaita, E., Khalil, I., Othman, N. S., Khreishah, A., & Guizani, M. (2019). Unmanned aerial vehicles (UAVs): A survey on civil applications and key research challenges. *IEEE Access*, *7*, 48572-48634. https://doi.org/10.1109/access.2019.2909530

Shmilovich, A., & Yadlin, Y. (2008). Flow control for the systematic buildup of high-lift systems. *Journal of Aircraft*, *45*(5), 1680-1688. https://arc.aiaa.org/doi/10.2514/1.35327

Shyy, W., Jayaraman, B., & Andersson, A. (2002). Modeling of glow discharge-induced fluid dynamics. *Journal of Applied Physics*, *92*, 6434-6443. https://doi.org/10.1063/1.1515103

Xu, X., & Zhou, Z. (2015). Study on longitudinal stability improvement of flying wing aircraft based on synthetic jet flow control. *Aerospace Science and Technology*, *46*, 287-298. https://doi.org/10.1016/j.ast.2015.07.022

Zhao, Z., Luo, Z., Deng, X., Zhang, J., Liu, J., & Li, S. (2023). Effects of dual synthetic jets on longitudinal aerodynamic characteristics of a flying wing layout. *Aerospace Science and Technology*, *132*. https://doi.org/10.1016/j.ast.2022.108043

Zhou, Y., Zheng, S., & Chang, J. (2022). Investigations on the interfering factor of single synthetic jet actuator on improving the efficiency of wing control surface. *Journal of Applied Fluid Mechanics*, *15*(6). https://doi.org/10.47176/jafm.15.06.1236